A Neural network model for the separation of atmospheric effects on attenuation: Application to frequency scaling.

Laurent Barthès, Cécile Mallet, O. Brisseau

A neural network model for the separation of atmospheric effects on attenuation: Application to frequency scaling

Laurent Barthes,[1] Cécile Mallet,[1] and Olivier Brisseau[2,3]

Received 1 July 2005; revised 3 April 2006; accepted 11 May 2006; published 1 August 2006.

[1] Attenuation due to the propagation of radio waves through the Earth's atmosphere plays a major role in satellite link attenuation at frequencies beyond 20 GHz. This paper presents the development of an artificial neural network (ANN) to separate out the respective roles played by the three types of contributor, namely, gases (oxygen and water vapor), clouds, and rain, to the overall attenuation of radio waves. Whereas the inputs to the ANN are the total attenuation measured at either one, two, or three frequencies, the ANN outputs provide the three atmospheric attenuation components at a single frequency. Several neural networks were trained by using a simulated statistically significant data set, derived from absorption and diffusion models applied to atmospheric profiles. Good overall performance was observed, and a particularly good fit was achieved in the case where attenuation inputs were provided at two frequencies. From the estimated values of atmospheric attenuation for the three contributors, corresponding frequency scaling models were applied on each to estimate the three contributions at a new frequency. Total atmospheric attenuation at this new frequency can then be estimated. The method works using measured data at either one, two, or three frequencies and allows the total attenuation to be predicted at any other frequency in the range 20–50 GHz. Validation was successfully performed on real data.

Citation: Barthes, L., C. Mallet, and O. Brisseau (2006), A neural network model for the separation of atmospheric effects on attenuation: Application to frequency scaling, *Radio Sci.*, *41*, RS4012, doi:10.1029/2005RS003310.

1. Introduction

[2] Atmospheric attenuation significantly affects radio wave propagation in satellite links operated in high-frequency bands, between 10 and 50 GHz. It is caused by several types of atmospheric component: gases (oxygen and water vapor), clouds and rain. Each of these components behaves quite differently, when considered in terms of its temporal and spatial variability. Moreover, the relative contribution of each component to the total attenuation varies with frequency.

[3] In the case of a satellite slant path, gaseous attenuation, due mainly to water vapor and oxygen, can exceed 3 dB at frequencies below 50 GHz and at low elevation angles. This form of attenuation can be considered to be homogeneous, over the horizontal range of a link. Liebe's model allows accurate modeling of gaseous attenuation up to 1000 GHz, by using vertical profiles of atmospheric parameters (temperature, pressure, humidity). For frequencies below 50 GHz, a water vapor absorption peak is observed near 22 GHz. Spatial and temporal variations in gas-induced attenuation are mainly due to spatiotemporal variations in water vapor quantity.

[4] Attenuation due to nonprecipitating clouds, composed of liquid water or ice particles, leads to a maximum of about 4 dB for low elevation angles at 50 GHz, and total cloud-induced attenuation increases nearly as the square of frequency. The Rayleigh approximation can be used to calculate its contribution at frequencies below 50 GHz, such that the resulting attenuation is proportional to the integrated liquid water content present along the link. As cloud coverage varies considerably in both the horizontal and vertical directions, and the corresponding liquid content varies substantially in space and time, cloud-induced attenuation can vary strongly.

[1]Centre d'Etude des Environnements Terrestre et Planétaires, Velizy, France.
[2]Institut d'Électronique et de Télécommunications de Rennes, Université de Rennes I, Rennes, France.
[3]Centre d'Électronique de l'Armement, Bruz, France.

0048-6604/06/2005RS003310

[5] Rain is the strongest contributor to attenuation in radio wave propagation at frequencies above 10 GHz. It increases with rainfall rate and frequency [*European Cooperation in the Field of Science and Technology* (*COST*), 1999b] and becomes particularly significant in V band (36 dB for a slant path at 50 GHz, for a rainfall rate of 50 mm/h). At any given frequency, rain-induced attenuation depends mainly on the shape and size distribution profile of the raindrops. In order to perform accurate rain attenuation calculations, a good knowledge is needed of these characteristics at each point along the link. The rain rate varies noticeably in space and time, and thus leads to particularly dynamic properties in the propagation channel. The present study concerns the range 20–50 GHz, which is roughly extends over the Ka and Q bands. Most of the statements and conclusions made in this paper are only valid within this frequency range.

[6] Satellite telecommunication systems using these frequency bands need to compensate for atmospheric attenuation. One of the fade mitigation techniques used to combat these phenomena is uplink power control. The transmission power is adjusted in accordance with the state of the atmosphere. As an example, it may need to be increased very quickly during rainy conditions. The uplink always uses a higher frequency band than the downlink, and is thus more sensitive to atmospheric effects. In practice, the required changes in uplink power are determined by scaling the attenuation measured in the downlink. The frequency scaling technique is based on the determination of a relationship between the attenuation occurring at two or more different frequencies. As the various atmospheric contributions behave differently as a function of frequency, each contributor generates a different frequency scaling ratio. In cases where one contributor is considerably more significant than the others (typically, during a strong rain event), the total scaling ratio is determined uniquely by that relevant to the main contributor. Consequently, in the case of very strong attenuation, the total scaling ratio can be approximated by the scaling ratio due to rain. However, if accurate attenuation frequency scaling is needed over a large range of attenuation and frequency values, as will be the case for new services which plan to use frequencies above 35 GHz, each of the individual atmospheric contributors will need to be accounted for. Under these conditions, a specific scaling ratio [*COST*, 1999a, 1999b] will be used for each of the atmospheric contributors, in order to determine an overall scaling ratio for the propagation channel in question.

[7] Separation of the different atmospheric contributions (also called separation effects) is an essential step in the study of the dynamics of the propagation channel. In addition, it is known that each of the atmospheric components is subject to temporal variations, which are individually specific. As a result, the prediction of global attenuation at time $t + \Delta T$, based on known attenuations at time t, will certainly be improved by considering separately the attenuation predictions of each contribution.

[8] Our aim in this paper is to present a statistical model able to separate out the respective roles played by the three types of atmospheric contributor. An artificial neural network (ANN) is trained to estimate the respective contributions from gases (oxygen and water vapor), cloud and rain, to the overall attenuation measured at one or more frequencies. This training is performed in a supervised manner, and involves the development of a training base. In this manner, a very large database containing the ANN input data and corresponding targets is simulated from a wide set of atmospheric profiles, corresponding to different sets of meteorological conditions. The first section of this paper deals with the development of ANN models and the development of the simulated database. The second section is devoted to the performance of different separation models on simulated and real measurements. Finally, in the third section, we apply the models to frequency scaling applications, and performance is assessed using attenuation measurements acquired during the Olympus experiment.

2. Development of a Neural Network Model for the Separation of Atmospheric Attenuation Effects

2.1. Methodology

[9] Several theoretical results have demonstrated the capacity of an ANN to perform well as a universal approximator [*Cybenko*, 1989; *Hornik et al.*, 1989]. ANNs are capable of learning from examples and do not require a priori assumptions about the function they approximate. The neural network described here is a multilayered perceptron (MLP). An MLP performs algebraic functions on its inputs, by combining the functions performed by its neurons. A neuron is a nonlinear, parametric and bounded, algebraic function defined by its state o_i, its connection weights w_{ij} to neurons located upstream, and its activation function f. It carries out the following operation:

$$o_i = f(s_i), \tag{1}$$

with

$$s_i = \sum_{j=1}^{n} w_{ij} o_j.$$

[10] The use of nonlinear activation functions f makes it possible to obtain nonlinear statistical models. Sigmoid

or hyperbolic tangents are generally used. An MLP is defined by its architecture and weights. In other words, it is characterized by its topology, namely, the number of inputs, outputs, hidden neurons and how they are interconnected. An MLP consists of successive layers (a layer is a set of nonconnected neurons). All connections are directed from lower to upper layers. Neurons of the first hidden layer compute their state from the inputs of the model affected by weights. Neurons of the next layer compute their state from the outputs of the previous layer affected by weights, and so on.

[11] The estimation of the weights, which constitutes the learning process, requires a database composed of a wide set of couples (X^j, Y^j), with j ranging from 1 and N, corresponding to the input-output data set of the system to be modeled by the ANN. In our case,

$$\begin{cases} X = \left[A_{f_1}\right] \text{ or } X = \left[A_{f_1}, A_{f_2}\right] \quad \text{or } X = \left[A_{f_1}, A_{f_2}, A_{f_3}\right] \\ Y_i = \left[\dfrac{A_{gaz\,f_i}}{A_{f_i}}; \dfrac{A_{cloud\,f_i}}{A_{f_i}}; \dfrac{A_{rain\,f_i}}{A_{f_i}}\right], \end{cases} \tag{2}$$

where A_{f_k} is the total attenuation at frequency f_k, and $A_{gaz\ f_i}$, $A_{cloud\ f_i}$, $A_{rain\ f_i}$ represent gas, cloud and rain attenuations at frequency f_i.

[12] Learning consists in determining the weights W by minimizing a cost function, that is, a measure of the mismatch between target values and predicted values. To approach the minimum of this multidimensional cost function a gradient technique is used, which is an iterative optimization method, adapted to the MLP by gradient back propagation [*Bishop*, 1995]. Cross-validation tests, based on a procedure referred to as the early stopping method of training [*Haykin*, 1999], allowed us to control the quality of the minimum estimation and of generalization. In practice, the database was divided randomly into three subsets (training 40%, cross validation (30%) and test (30%)). The first subset was devoted to the learning step, the second was used to find the best ANN architecture, that is, the architecture providing the best performance using this subset (number of layers, number of neurons per layer), and the third was then used to compute the ANN performance discussed in the present paper.

[13] In order to ensure that the sum of the different effects remains equal to the total attenuation, an output layer neuron of the MLP must have the following properties:

$$\sum_{j=1}^{3} Y[j] = 1 \quad \text{and} \quad 0 \le Y[j] \le 1. \tag{3}$$

[14] These constraints can be satisfied by choosing to relate the network's outputs s_j by a softmax function. This activation function is generally used to estimate a posteriori probabilities, and in this case it is highly desirable for those outputs to be positive, and for their sum to be 1. The role of the softmax activation function is to enforce these constraints on the outputs [*Bridle*, 1990]:

$$Y[j] = \frac{\exp(s_j)}{\sum_{k=1}^{3} \exp(s_k)}. \tag{4}$$

2.2. Training Databases

[15] As explained in section 2.1, the ANN must be trained to process inputs, before they can be used in a given application. As it is not possible to make direct measurements of the individual atmospheric attenuation contributions, this problem has to be tackled using simulated data. It is thus a matter of computing results from a very large database. For this purpose, a wide set of atmospheric profiles was made available to our team by the European Centre for Medium Weather Forecast (ECMWF). Initially, the data set included more than 10^6 data points, corresponding to the 36-hour forecast experiment performed on several dates in 2003. Each data point contains temperature, pressure, moisture, cloudy liquid water, cloud cover, precipitating rain and ice profiles, for 60 altitudes between ground level and 30 km. Within each atmospheric profile, the coherence of the different fields (water vapor, cloud and rain) is ensured by the quality of the atmospheric model and by the assimilation process incorporating real data into the model. A variety of atmospheric conditions is ensured by using data corresponding to a wide range of geographic situations, representative of all continental surfaces lying at latitudes in the interval ±70°. The spatial resolution of the data set, equivalent to 1 point per 40 km^2, was found to be too coarse for our purposes. In particular, rain quantities are underestimated relative to observed quantities on a ground-satellite link. Specific processing, described in a previous paper [*Barthes et al.*, 2003], was thus carried out in order to obtain a statistically representative subset. By considering the atmosphere to be horizontally stratified, the extinction of each layer is computed to give the atmospheric attenuation after integration.

[16] In the case of gas-induced attenuation, the extinction coefficient is equal to the absorption coefficient: $k_{gaz\ f}(z) = k_{oxygen\ f}(z) + k_{watervapor\ f}(z)$ [dB/km]. The superiority of Liebe's microwave propagation model [*Liebe et al.*, 1993] was recognized [*COST*, 1999a] for computing the gas absorption of each atmospheric layer. For clouds, the extinction $k_{cloud\ f}(z)$ at height z and

frequencies below 60 GHz resulting from scattering is negligible, so that the extinction coefficient can be computed using Rayleigh's theory [*Liebe et al.*, 1993].

[17] In the case of rain, the relationship between the microphysical properties of rain and the attenuation observed at a given frequency f depends on elevation angle and polarization. In fact, the extinction cross section of a particle in air depends on four main parameters: the elevation angle under consideration, the complex refractive index of water, the shape of the particle and its electromagnetic size $\chi = (2\pi/\lambda)r$, where r is the equivalent radius of the particle and λ the wavelength. As shown in a previous study [*Brisseau et al.*, 2003], the main effect is the drop size distribution. In general, the shape of rain droplets needs to be taken into account in the case of heavy rain rates and low elevation angles. However, in this study only spherical drops were considered because drop shape has only a slight effect in the simulation of light rain. In the case of simulations involving heavy rain, the influence of drop shape was considered to be secondary, when compared with the difficulty of separating out the effects of light rain and cloud.

[18] When the raindrops are assumed to be spherical, there is no dependence on elevation angle or polarization, and the extinction cross section of each drop depends only on its size. We define $N(D, z)$ (in m^{-4}) as the raindrop size distribution (DSD) prevailing in the atmosphere at altitude z, that is, the number of drops per cubic meter per unit increment of diameter D. The rain specific attenuation $k_{rain\,f}(z)$ (in dB/km) is then given in dB/km by

$$k_{rainf}(z) = 4343 \int_{D_{\min}}^{D_{\max}} N(D,z)\sigma_{f_{ext}}(D)dD, \qquad (5)$$

where $\sigma_{f_{ext}}(D)$ (in m^2) is the extinction cross section for a raindrop of diameter D (in m) computed using Mie's theory (assuming spherical drop shapes). In the atmospheric profile data sets, only the rain rate corresponding to each atmospheric layer is provided. Certain assumptions thus need to be made concerning the rain particle microphysics. We use three different DSDs: the Joss convective and stratiform laws for particle size distribution [*Joss et al.*, 1968] represent "extremes" in terms of rain regime, whereas the Marshall Palmer law [*Marshall and Palmer*, 1948] represents a mean rain DSD. A rainy situation within the data set is thus associated with a set of three rain extinction coefficients, corresponding respectively to the above DSD laws, leading to three rain specific attenuations values.

[19] The atmospheric attenuation of the different effects is then obtained after integration along the vertical atmospheric profile. The total atmospheric attenuation is the sum of the different effects (in dB):

$$\left.\begin{aligned} A_{gazf} &= \int_0^H k_{gazf}(z)dz \\ A_{cloudf} &= \int_0^H k_{cloudf}(z)dz \\ A_{rainf} &= \int_0^H k_{rainf}(z)dz \end{aligned}\right\} A_f = A_{gazf} + A_{cloudf} + A_{rainf}. \qquad (6)$$

[20] The data set $\{(X^k, Y^k)$ with $k = 1, \ldots, N\}$, where X and Y are defined in equation (2), is then computed over the full extent of the profiles and for the three DSDs defined above, for the range of frequencies ($f \in [10, 50]$ GHz). All simulations, and thus all MLP models presented in the following, are made assuming zenith angle attenuation. The attenuation $A_f(\theta)$ observed at an elevation angle θ can be computed from the zenith attenuation using $A_f = A_f(\theta).\sin(\theta)$. The validity range of the model is limited by the latter relationship because of the limited extent of rain cells. In the case of very low elevation angles ($\theta < 10°$), the relative influence of the different attenuation contributors is not the same as at higher elevations, and the proposed model will in this case overestimate the rain contribution.

3. Performance of the Separation Model

3.1. Performance Using the Test Database

[21] An optimal MLP model was obtained using training and a cross-validation database. By using the early stopping method, an architecture based on two hidden layers and seven neurons per layer was implemented. The performance presented in this section is computed from the third part of the data set (test database). In this paper only those results corresponding to $f_1 = 20$ GHz, $f_2 = 30$ GHz and $f_3 = 40$ GHz are presented. These frequencies were used in the Olympus and Italsat experiments, thus allowing a comparison between measurements and the results of the present model, as described in section 3. Figures 1a, 1b, and 1c show the different components of the vector $Y = [A_{gaz\,f_1}/A_{f_1}; A_{cloud\,f_1}/A_{f_1}; A_{rain\,f_1}/A_{f_1}]$, respectively, as a function of A_{f_1} ($f_1 = 20$ GHz), used in the training database. In the case of low levels of attenuation, gas is the main contributor, whereas in the case of strong attenuation, the relative contribution from gases is less than 10%. Inversely, the rain contribution increases from 0 to 92% when total attenuation

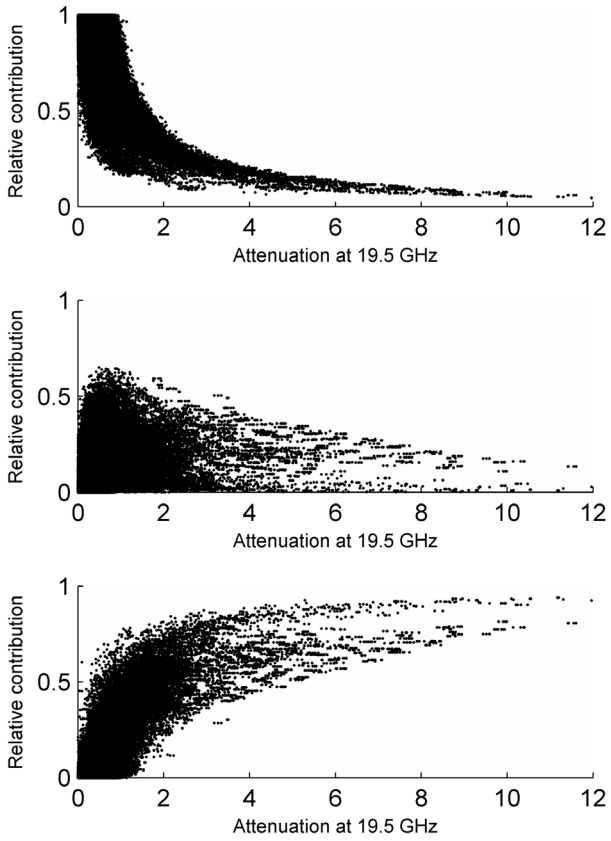

Figure 1. Training database used to train the neural network models. Relative contributions are shown as a function of equivalent zenith attenuation at a frequency of 19.5 GHz for the case of (a) gases, (b) clouds, and (c) rain.

increases from low to very high levels. Three different neural network models were developed to estimate Y from the total attenuation measured at one, two or three frequencies.

[22] Figure 2 shows the results obtained with these different neural network models corresponding to one, two or three inputs: $\hat{Y}_1 = F_1(W, X = [A_{f_1}])$; $\hat{Y}_1 = F_{12}(W, X = [A_{f_1}, A_{f_2}])$; $\hat{Y}_1 = F_{123}(W, X = [A_{f_1}, A_{f_2}, A_{f_3}])$. It can be seen that the mean behavior of the three models is approximately the same. The main difference between the three results is the fidelity with which, at any given attenuation level, the intrinsic variability of the contributions is represented. As could be expected, when the number of inputs is increased, the improved accuracy of the model reveals the variability of the contributions. Concerning the relative contributions of gases $Y[1]$, good performance is observed for clear sky conditions, with an estimated relative contribution close to 1. Discrepancies are however observed, which tend to decrease with the number of inputs. Comparison of the expected cloud contributions $Y[2]$ and $\hat{Y}[2]$ shows in the three models a saturation phenomenon observed for A_{f_1} close to 1 dB. Indeed, the maximum value is 0.24 for F_{123} and F_{12}, and 0.2 for F_1, when the relative attenuation contribution from the clouds reaches 0.6 in the simulated database. This phenomenon is mainly due to the difficulty in distinguishing small rain events from cloud situations.

[23] Figure 3 provides a comparison between the expected relative rain contributions $Y[3]$ and the values $\hat{Y}[3]$ obtained using the three models. As most of the data corresponds to clear sky situations, that is, with rain contributions equal to zero, the neural network models easily learn how to behave under these conditions. Conversely, the scarcity of intense rain data makes it more delicate for the neural network to learn the behavior of high relative rain contributions. The models F_{12} and F_{123} present very similar performances, and it can be seen that the addition of a third frequency (39.6 GHz) brings no significant improvement to the separation. The single-frequency model F_1 shows poorer performance, with systematically underestimated relative contributions in the case of heavy rain.

3.2. Performance With Real Data

[24] The Olympus data set consists of measurements of total attenuation at 20 and 30 GHz at 1-s time intervals, recorded from May to October 1992. The neural network models cannot be validated directly from real data recorded during the propagation experiment, since it is not possible to collect separate direct measurements of the different contributions. The model can however be partially validated using the method described in the following: we consider the coherence of different outputs to be guaranteed by equation (4), such that the validation of one contribution leads to a good degree of confidence in the overall performance of the model. The frequency scaling coefficient for cloud attenuation ($r_{cloud\ f2/f1} = A_{cloud\ f_2}/A_{cloud\ f_1}$) is independent of liquid water content in cloud [*COST*, 1999a] and, contrary to the gas or rain scaling coefficients, is nearly constant for a given set of frequencies. Only variations in cloud temperature profiles can lead to small variations in this coefficient. As an example, for $f_1 = 20$ GHz and $f_2 = 30$ GHz, the cloud frequency scaling coefficient can vary (according to cloud temperature profile) between 2 and 2.5, with a mean and most probable value equal to 2.25. Two different single-frequency separation models $\hat{Y}_1 = F_1(W, X = [A_1])$ and $\hat{Y}_2 = F_2(W, X = [A_2])$ were applied to attenuation measurements during the five months of the Olympus campaign, and the corresponding cloud scaling coefficients were then computed as $\hat{r}_{cloud\ f2/f1} = \hat{A}_{cloud\ f_2}/\hat{A}_{cloud\ f_1} = \hat{Y}_2[2]/\hat{Y}_1[2]$. The same mean value (2.25) is obtained with variations between 1.7 and 2.4.

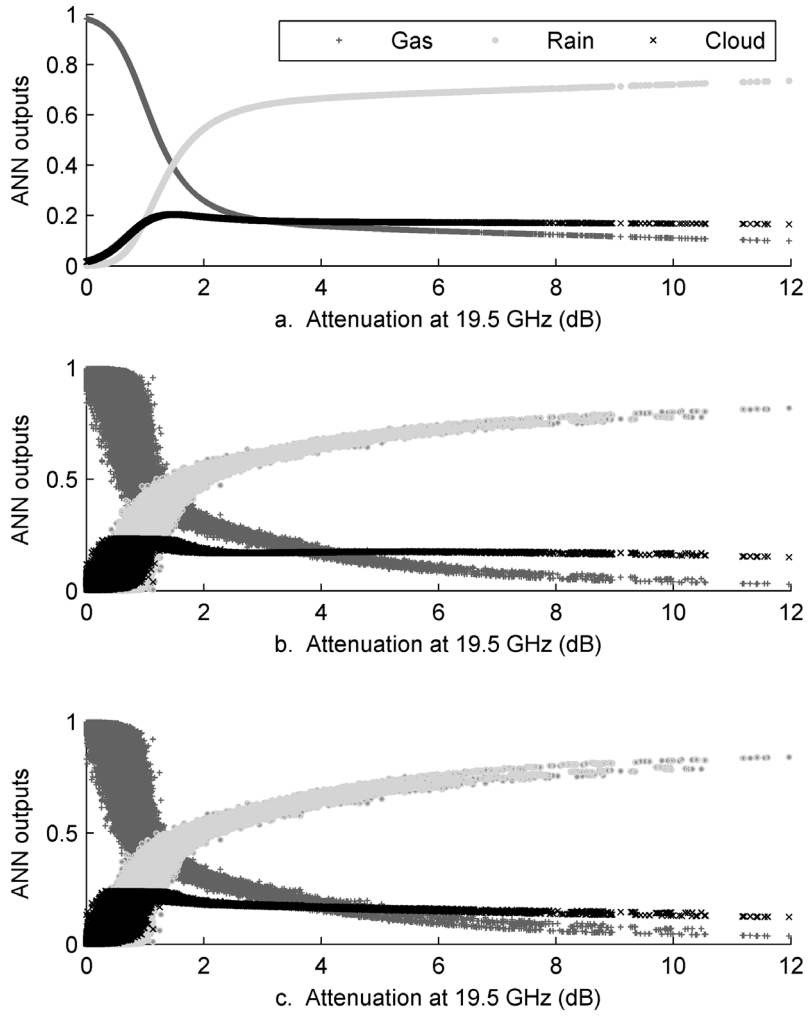

Figure 2. Estimated relative contributions of gas, cloud, and rain as a function of equivalent zenith attenuation at a frequency of 19.5 GHz: (a) one input (F_1 model), (b) two inputs (F_{12} model), and (c) three inputs (F_{123} model)).

Whereas the above description shows that there is good partial validation for the cloud component, it appears reasonable to assume that the use of equation (4) will ensure good agreement for the other two components. A second validation approach, based on frequency scaling, is described in section 3.

4. Application to Scaling Frequency of Total Attenuation

4.1. Methodology

[25] Section 2 describes how the different atmospheric contributions can be separated at a given frequency f_1. As these contributions will lead to different frequency scaling ratios, specific scaling frequency ratios need to be applied to each of the attenuation components, in order to estimate their respective attenuation contributions at a new frequency f_2. The total attenuation at f_2 can then be derived from the new set of attenuation contributions. Figure 4 illustrates the different steps leading to the estimation of overall attenuation at frequency f_2 on the basis of attenuation measurements at a generally lower frequency f_1.

[26] A new model for the frequency scaling of rain, based on its microphysical characteristics, has recently been developed and published [*Brisseau et al.*, 2005, 2006]. This model was used in the present study for

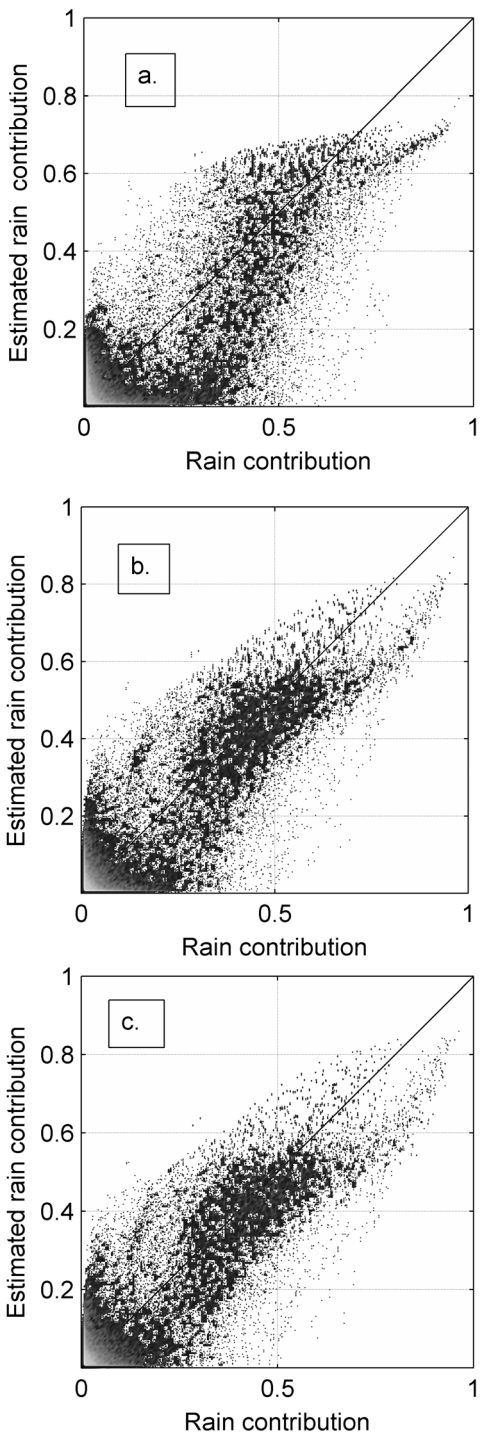

Figure 3. Model-estimated relative contributions of rain $\hat{Y}[3]$ as a function of expected relative contributions $Y[3]$ for three models: (a) F_1, (b) F_{12}, and (c) F_{123}.

the frequency scaling of rain. The COST model allows atmospheric attenuation due to oxygen and water vapor to be computed, at any frequency, from ground-based pressure, temperature and humidity measurements. It can thus be used to obtain the scaling ratio, between any pair of frequencies, for the gas contribution. The COST model also allows cloud liquid attenuation to be computed at any frequency, from temperature and cloud liquid water content. It can also be used to obtain the scaling ratio for cloud as a function of temperature only (because the ratio is independent of cloud liquid content).

4.2. Results on Simulated Data

[27] The methodology previously described is applied for f_1 = 20 GHz; f_2 = 40 GHz. Estimated attenuations $\hat{A}_{40} = f(A_{20}P, T, H)$ are compared with A_{40} simulated directly from the atmospheric profiles (Figure 5a). Similarly, by using a two frequency neural network model $F_{12}(W, X = [A_{f_1}, A_{f_2}])$ instead of $F_1(W, X = [A_{f_1}])$, attenuation at a third frequency can be estimated using the scaling models. This second methodology is also applied for f_1 = 20 GHz; f_2 = 30 GHz; f_3 = 40 GHz, and estimated values of $\hat{A}_{40} = f(A_{20}, A_{30}, P, T, H)$ are compared with the attenuation A_{40} simulated directly from the atmospheric profiles (Figure 5b). It can be seen that the standard deviations are substantially reduced, especially for attenuations greater than 8 dB. Overall performance based on simulated data is thus encouraging. A mean error of 0.1 dB for all attenuation levels, and a maximum mean error of less than 1 dB for attenuations greater than 10 dB are obtained. The standard deviation increases with attenuation, reaching 1 dB for an attenuation of 20 dB. Its average value over the range of simulated attenuations is 0.23 dB.

4.3. Validation Based on Olympus Experiment Data

[28] In this section we describe how the previously described methodology has been applied to real data at f_1 = 20 GHz, f_2 = 30 GHz, enabling estimated attenuations $\hat{A}_{30} = f(A_{20}, P, T, H)$ to be compared with direct measurements of A_{30}. Figure 6 provides an example of the different atmospheric contributions obtained with the neural network model, and compares the estimated and measured attenuations at 30 GHz. It can be observed that gas attenuation is relatively stable, even when the total attenuation is very high. Cloud and rain attenuations are close to zero for small global attenuation levels corresponding to clear sky conditions. A very good agreement is observed between estimated and measured 30 GHz attenuations, with only a small underestimation occurring at attenuations higher than 20 dB. The 30 GHz attenuation mean error (bias) and standard deviation are computed

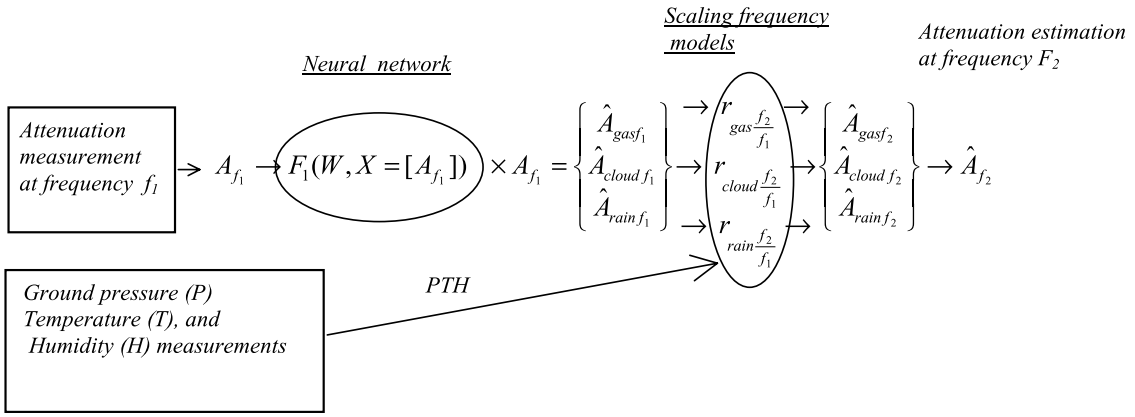

Figure 4. Block diagram of the total attenuation frequency scaling algorithm using a single-frequency neural network model.

as a function of attenuation. A maximum of 0.7 dB bias and 2 dB standard deviation are observed for attenuations higher than 18 dB. For attenuations lower than 10 dB the bias is less than 0.4 dB and the standard deviation is less than 0.8 dB.

[29] Figure 7 illustrates attenuation excess probabilities for three different frequencies, expressed as the percentage of total measurement time (here, the data was collected over a period of five months) during which any given level of attenuation is exceeded. For the case of 30 GHz, excess probabilities from real and estimated data are compared, and found to be in very good agreement. This result is deemed to validate the MLP separation models and the scaling models at 20 GHz and 30 GHz.

[30] Although no direct validation can be performed at other frequencies, the good agreement observed for the Olympus campaign frequencies provides a priori validation of the data sets used to develop the different models. As the atmospheric profiles and attenuation models used are identical for all frequencies, this partial validation is evidence that the results obtained are also relevant to the other channels.

4.4. Frequency Scaling From the Olympus Experiment to 44 GHz

[31] Following validation with Olympus experimental data, the method described above can be used to improve our knowledge of the behavior of propagation channels in higher frequency bands. Attenuation time series or statistics at any frequency below 50 GHz can be obtained from measurements carried out during the Olympus or Italsat experiments. In anticipation of certain applications making use of the Syracuse III

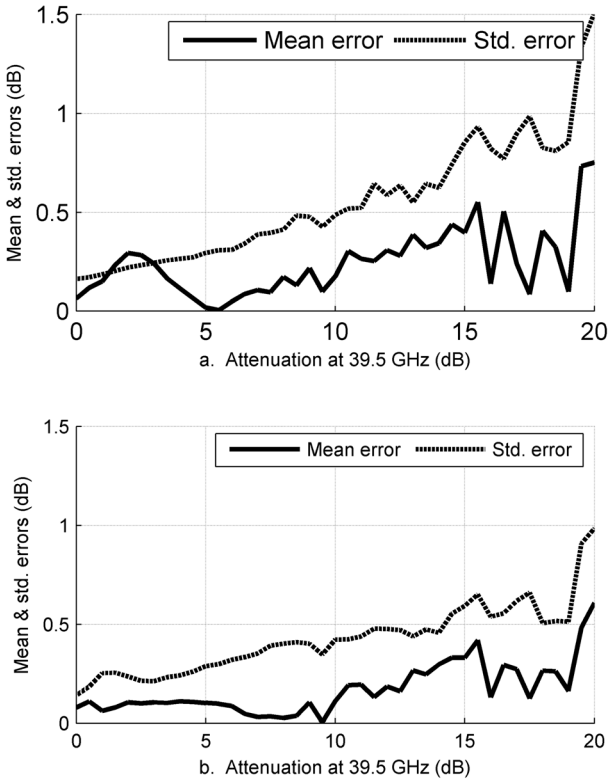

Figure 5. Mean 39.5 GHz attenuation error (bias) and standard deviation as a function of 40 GHz attenuation for the (a) F_1 model (one input) and (b) F_{12} model (two inputs)).

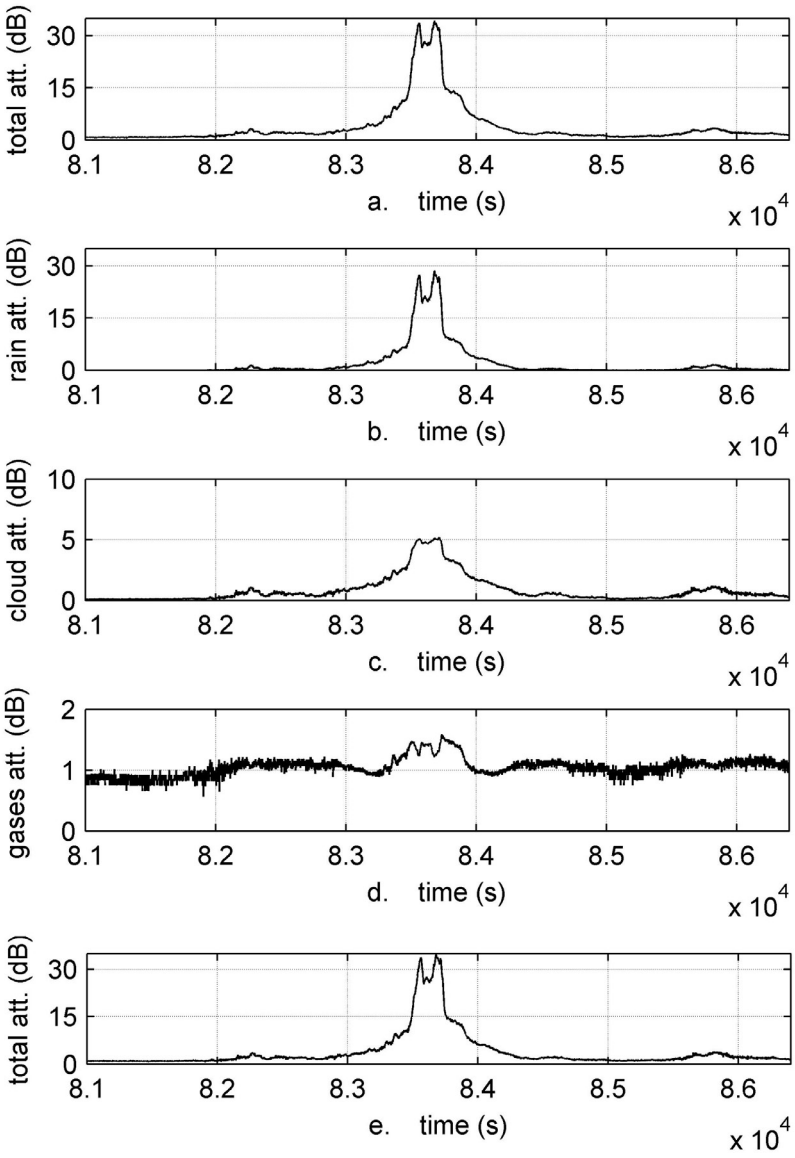

Figure 6. Olympus propagation measurements carried out on 28 August 1998 at Gometz-la-ville (France): (a) measured 30 GHz attenuation; corresponding (b) rain, (c) cloud, and (d) gas contributions; and (e) total attenuation, derived from the neural network at 30 GHz.

military satellite communications system, simulations were made of the propagation channel behavior at 44 GHz, for an elevation angle of 30°.

[32] The methodology previously described was applied for f_1 = 20 GHz; f_2 = 30 GHz; f_3 = 44 GHz, and Olympus measurements were used to estimate $\hat{A}_{44} = F_{12}(A_{20}, A_{30}, P, T, H)$. Figure 8 provides a sample attenuation time series, corresponding to the same event as that presented in Figure 6, at 20 and 30 GHz. Very strong temporal gradients peaking at 0.6 dB/s can be observed, as opposed to gradients of only 0.13 dB/s for the same time series at 20 GHz. In this particular example, the rain contribution alone reached a level of 50 dB. Even higher levels of rain attenuation can occur at this frequency.

[33] Figure 7 illustrates the corresponding attenuation excess statistics, which demonstrate the importance of designing fade mitigation techniques into a

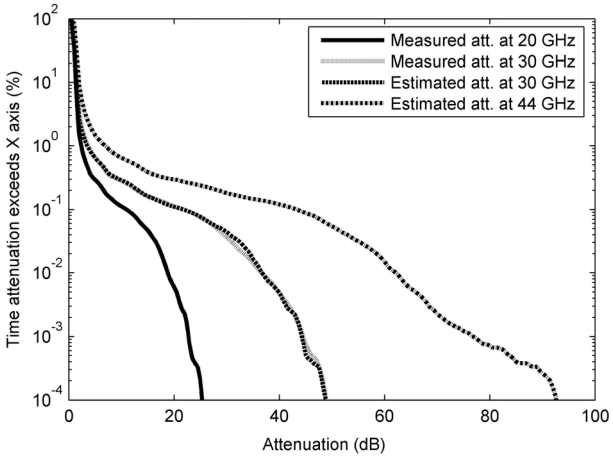

Figure 7. Attenuation excess probabilities at 20 GHz (measured), 30 GHz (measured and estimated), and 44 GHz (estimated).

static margin system, since the margin needed to ensure quasi permanent link availability would be prohibitive.

5. Conclusion

[34] At frequencies below 18 GHz, rain is the main contributor to the total attenuation of a radio frequency link. This is the reason for which, until recently, only rain was taken into account in frequency scaling models. However, as new telecommunication systems tend to use frequencies above 20 GHz, the attenuation contributions of gases and clouds can no longer be neglected. As a result, specific frequency scaling ratios must be applied to each contribution in order to derive the total atmospheric attenuation at a new frequency. Preliminary separation of the three different atmospheric contributions is essential to accurate frequency scaling estimations. In the present paper, a method based on neural networks has been developed to separate out the different contributions. Partial validation on real measurements has given us considerable confidence in the model's performance over the [20–50] GHz frequency interval. An example of frequency scaling is given, in which the dynamics and statistical properties of attenuation are derived for the 44 GHz channel, from measurements at 20 and 30 GHz.

[35] Because the different atmospheric components are characterized by quite different spatiotemporal dynamic behaviors, the separation models could be used to improve predictive attenuation models on the basis of prior attenuation measurements at the same or lower frequencies.

[36] At the present time, our neural models use either one, two or three attenuation measurements as input. By making use of conventional ground level meteorological measurements such as pressure, temperature and humidity, these models could certainly be improved. Although more sophisticated measurements such as accurate radiometric determinations of sky brightness temperature are currently rather delicate and expensive to implement, they have the potential of enabling much improved separation of the specific contributions to global atmospheric attenuation.

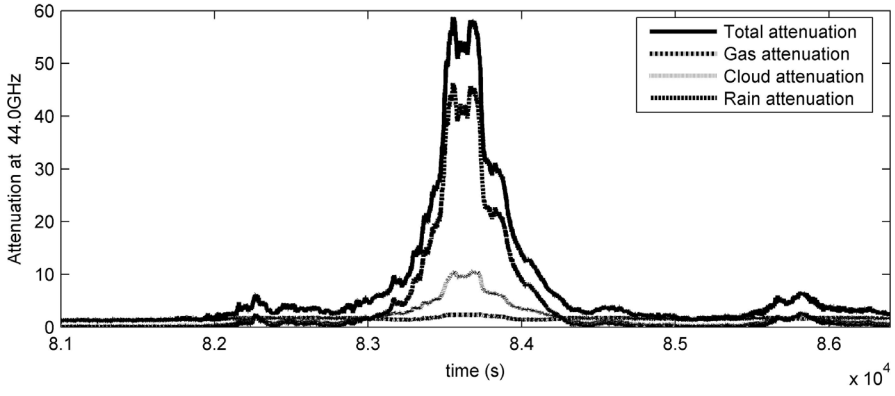

Figure 8. Attenuation time series simulation at 44 GHz, derived from Olympus measurements made on 28 August 1992 at Gometz-la-ville (France): Total attenuation and corresponding gas, cloud, and rain contributions are presented.

[37] **Acknowledgments.** This work was supported by CELAR. Thanks are also due to T. Marsault for support of this collaboration.

References

Barthes, L., C. Mallet, and P. Gole (2003), Neural network model for atmospheric attenuation retrieval between 20 and 50 GHz by means of dual-frequency microwave radiometers, *Radio Sci.*, *38*(5), 1082, doi:10.1029/2002RS002813.

Bishop, C. (1995), *Neural Networks for Pattern Recognition*, Oxford Univ. Press, New York.

Bridle, J. S. (1990), Probabilistic interpretation of feedforward classification network outputs, with relationships to statistical pattern recognition, in *Neuro-computing: Algorithms, Architectures, and Applications*, edited by F. F. Soulie and J. Herault, pp. 227–236, Springer, New York.

Brisseau, O., L. Barthes, and C. Mallet (2003), Effect of microphysical characteristics of rain on frequency scaling in microwave band, paper presented at IEEE International Geoscience and Remote Sensing Symposium, Inst. of Electr. and Electron. Eng., Toulouse, France, 21–25 July.

Brisseau, O., C. Mallet, L. Barthes, and T. Marsault (2005), Rain frequency scaling model using the normalized DSD concept, paper presented at European Conference on Propagation and Systems, Delegation Gen. pour l'Armement, Brest, France, 15–18 Mar.

Brisseau, O., C. Mallet, L. Barthes, and T. Marsault (2006), Frequency scaling of rain attenuation based on microphysical characteristics for SatCom links, *IEE Proc., Part H Microwaves Antennas Propag.*, in press.

Cybenko, G. (1989), Approximation by superpositions of sigmoidal function, *Math. Control Signals Syst.*, *2*(4), 303–314.

European Cooperation in the Field of Science and Technology (COST) (1999a), Final report on propagation effects due to atmospheric gases and clouds, in *Radiowave Propagation Modelling for SatCom Services at Ku-Band and Above*, edited by R. A. Harris, *Action 255*, chap. 2.1, pp. 2.1.1–2.1.41, Eur. Comm., Luxembourg.

European Cooperation in the Field of Science and Technology (COST) (1999b), Final report on rain attenuation, in *Radiowave Propagation Modelling for SatCom Services at Ku-Band and Above*, edited by R. A. Harris, *Action 255*, chap. 2.2, p. 2.2.79, Eur. Comm., Luxembourg.

Haykin, S. (1999), *Neural Networks: A Comprehensive Foundation*, Prentice-Hall, Upper Saddle River, N. J.

Hornik, K., M. Stinchcombe, and H. White (1989), Multilayer feedforward networks are universal approximators, *Neural Network*, *2*, 359–366.

Joss, J., J. C. Thams, and A. Walvoguel (1968), The variation of rain drop-size distributions at Locarno, paper presented at International Conference on Cloud Physics, Am. Meteorol. Soc., Toronto, Ont., Canada.

Liebe, H. J., G. A. Hufford, and M. G. Cotton (1993), Propagation modeling of moist air and suspended water/ice particles below 1000 GHz, paper presented at AGARD 52nd Specialists Meeting of Electromagnetic Wave Propagation, Advis. Group for Aerosp. Res. and Dev., Palma de Mallorca, Spain, 17–21 May.

Marshall, J. S., and W. M. K. Palmer (1948), The distribution of rain drops with size, *J. Meteorol.*, *5*, 165–166.

L. Barthes and C. Mallet, Centre d'Etude des Environnements Terrestre et Planétaires, 10-12 avenue de l'Europe, F-78140 Vélizy, France. (laurent.barthes@cetp.ipsl.fr; cecile.mallet@cetp.ipsl.fr)

O. Brisseau, CELAR, Route de Laillé, BP 5 7419, F-35174, Bruz, France. (olivier.brisseau@celar.fr)